Adv. Theor. Appl. Mech., Vol. 3, 2010, no. 8, 349 - 367

Singular Stress Fields for Transverse Cracks in Multi-Layer Satin Woven CFRP Composite Laminates under Cryogenic Conditions

Shinya Watanabe, Yasuhide Shindo*, Tomo Takeda and Fumio Narita

Department of Materials Processing, Graduate School of Engineering, Tohoku University, Aoba-yama 6-6-02, Sendai 980-8579, Japan
* shindo@material.tohoku.ac.jp

Abstract

The objective of this research is to analyze the singular stresses at the tips of cracks in multi-layer woven carbon fiber reinforced polymer (CFRP) composite laminates under tension at cryogenic temperatures. It is assumed that cracks appear in the transverse fiber bundles. We consider both cases where the tips of the cracks are located in the fiber bundles or at the interfaces between two fiber bundles. The generalized plane strain finite element analysis is carried out for the cracked woven CFRP laminates. Numerical results are expressed in terms of the stress intensity factor, and discussed in detail.

Keywords: Fracture Mechanics, Finite Element Method, Composite Material, Stress Intensity Factor, Thermal Stress, Cryogenics

1 Introduction

Woven carbon fiber reinforced polymer (CFRP) composites, due to their high stiffness to weight ratio and strength to weight ratio, have been considered as candidate materials for cryogenic fuel tank structures in future space vehicles [1]. Cryogenic fuel tanks receive mechanical and thermal loadings [2], and residual thermal stresses develop in the composites at cryogenic temperatures due to difference in the thermoelastic properties between the composite constituents. When residual thermal stresses are combined with stresses induced by mechanical loads, microcracks may initiate and propagate in the composites. These microcracks can act as passages for the cryogenic fuel to permeate,

which could ultimately lead to the failure of the whole structure [3]. Hence, it is very important to understand the fracture behavior of woven CFRP composites at cryogenic temperatures before they are used in cryogenic storage systems. Normal stresses at a crack tip are governed by stress singularity and stress intensity factor, and the evaluation of stress intensity factor is expected to offer a basic understanding of the crack behavior in composite materials.

With regard to numerical analysis, the presence of the undulation regions in woven composites leads to considerable complexities in the associated modeling, especially in comparison to composites based on non-woven reinforcement. As a result, numerical studies on the stress intensity factors for cracks in woven composites are still limited. In addition, woven composites are most frequently used by employing multiple layers of material to form a laminate, and interactions with adjoining layers and the free surface of the laminates can have a significant influence on the crack behavior in woven laminates. Therefore, the in-depth studies on these issues are important.

The purpose of this paper is to examine the singular stresses at the crack tip in multi-layer woven CFRP composite laminates under tension at cryogenic temperatures. Cracks are located in the fiber bundles, whose fibers are oriented perpendicularly to the mechanical load. Two-dimensional finite elements under generalized plane strain conditions are used to model the plane section of a laminate. Special elements with exact stress singularity are placed around the crack tip. Numerical results for the stress intensity factors are obtained and discussed.

2 Geometry of Cracked Woven Composite Laminates

The material investigated in this study is a five harness satin (5HS) woven composite laminate. The fiber reinforcement is a T800H carbon fabric (Toray Industries, Inc., Japan), and the matrix is a 3633 toughened epoxy resin (Toray Industries, Inc., Japan). The T800H/3633 5HS woven laminates have been developed for cryogenic fuel tanks [1]. Figure 1 shows the symmetrically stacked $2N$-layer 5HS woven laminates with cracks ($N = 1, 2, 3, ...$) in the Cartesian coordinate system O-xyz. The generalized plane strain condition is assumed. The woven composite laminates of thickness $4Nh$ comprise the warp and fill fiber bundles and the pure matrix, and are of infinite extent in the x-direction. The thickness of the warp and fill fiber bundles is h, and the width of the fiber bundles is l. We assume that the undulation angles are θ and $-\theta$.

Suppose that the satin woven composite laminates are subjected to the mechanical mean stress σ^*_{xx} in the warp direction (i.e. x-direction) and the thermal load of $\Phi - \Phi_s$, where Φ is the temperature of the composite laminates

and Φ_s is the temperature at the thermal stress-free state. Based on the experimental observations [4], a sufficiently large tensile stress in the warp direction leads to crack formation in the fill fiber bundles. In addition, the cracks initiate at undulations and where the fill fiber bundles are of the greatest thickness [5]. Thus, internal and edge cracks are located in $x = \pm 5nl$ planes ($n = 0, 1, 2, ...$) of the fill fiber bundles. The lengths of the internal and edge cracks are $2a$ and a ($a \leq h$), respectively. We consider two cases (Cases 1 and 2), and the crack locations for Cases 1 and 2 are as follows:

Case 1

$$\left.\begin{array}{ll} 2(k-1)h \leq |z| \leq 2(k-1)h + a & \text{for odd number of } k \ (k = 1, 3, 5, ...) \\ 2kh - a \leq |z| \leq 2kh & \text{for even number of } k \ (k = 2, 4, 6, ...) \end{array}\right\}, \quad (1 \leq k \leq N),$$

Case 2

$$\left.\begin{array}{ll} 2kh - a \leq |z| \leq 2kh & \text{for odd number of } k \ (k = 1, 3, 5, ...) \\ 2(k-1)h \leq |z| \leq 2(k-1)h + a & \text{for even number of } k \ (k = 2, 4, 6, ...) \end{array}\right\}, \quad (1 \leq k \leq N).$$

The surface layers of the woven laminates with an odd number of N for Case 1 and an even number of N for Case 2 contain the internal cracks, and those of the woven laminates with an even number of N for Case 1 and an odd number of N for Case 2 contain the edge cracks.

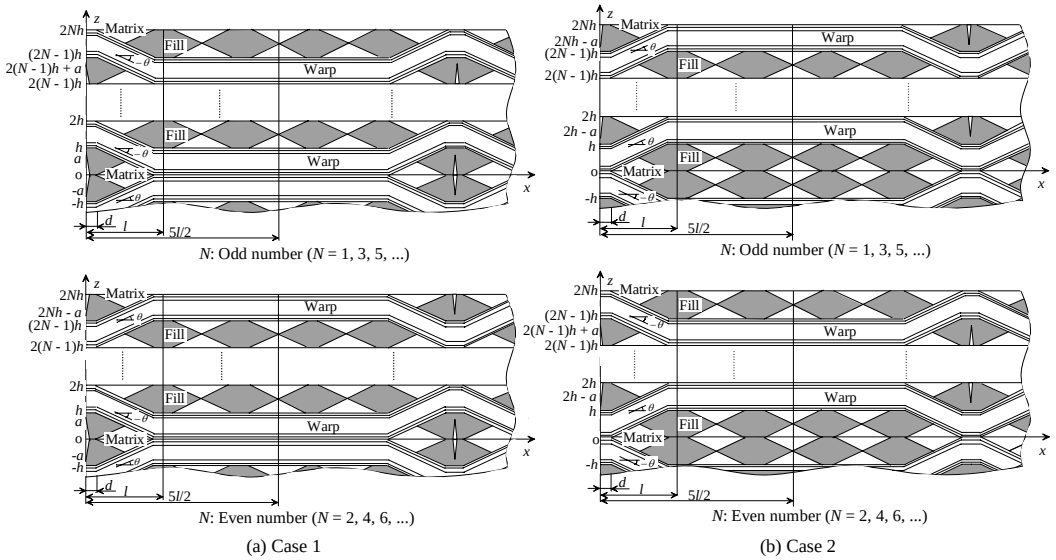

Figure 1 $2N$-layer five harness satin woven laminates with cracks ($N = 1, 2, 3, \ldots$).

3 Temperature-Dependent Material Properties

The material properties of the 3633 toughened epoxy resin matrix are taken to be isotropic and temperature dependent. The property data for the 3633 toughened epoxy resin are very difficult to find. Therefore, the Young's modulus $E_M(\Phi)$, Poisson's ratio $\nu_M(\Phi)$, shear modulus $G_M(\Phi)$ and coefficient of thermal expansion $\alpha_M(\Phi)$ of the matrix are assumed to be the same as those of the bisphenol-A epoxy resin. The subscript M denotes the matrix. The elastic and thermal properties of the bisphenol-A epoxy resin are approximated by the exponential functions of temperature [6] using the experimental data [7].

We assume temperature independent properties for the T800H carbon fiber, and the carbon fiber can be regarded as transversely isotropic material with Young's moduli E_{LF}, E_{TF}, Poisson's ratio ν_{LTF}, shear moduli $G_{LTF} = G_{TLF}, G_{TTF}$ and coefficients of thermal expansion α_{LF}, α_{TF}. The subscript F refers to the fiber, and the L and T denote the longitudinal and transverse directions, respectively. The first subscript on Poisson's ratio ν_{LT} refers to the direction of the applied tensile (compressive) stress, and the second subscript refers to the direction of the contraction (expansion). Only Young's modulus E_{LF} and coefficient of thermal expansion α_{LF} of the T800H carbon fiber are found in published data, and the remaining properties are assumed to be the same as the T300 carbon fiber properties [8]. A summary of the carbon fiber properties used in the analysis is given in Table 1.

The fiber bundles are considered as transversely isotropic unidirectional T800H/3633 composites. The composite cylinder assemblage (CCA) model [9] is used to predict the elastic and thermal properties of the fiber bundles $E_L^B(\Phi)$, $E_T^B(\Phi)$, $\nu_{LT}^B(\Phi)$, $G_{LT}^B(\Phi) = G_{TL}^B(\Phi)$, $G_{TT}^B(\Phi)$, $\alpha_L^B(\Phi)$, $\alpha_T^B(\Phi)$ in terms of the bundle constituent properties and the fiber volume fraction in the fiber bundles V_F^B. The superscript B denotes the fiber bundle.

Table 1 Elastic and thermal properties of carbon fiber

E_{LF} (GPa)	E_{TF} (GPa)	ν_{LTF}	G_{LTF} (GPa)	G_{TTF} (GPa)	α_{LF} (10^{-6}/K)	α_{TF} (10^{-6}/K)
294	40.0*	0.26*	24.0*	14.3*	−0.56	10.0*

* Property data for the T300 carbon fiber [8]

4 Finite Element Analysis

The constitutive equations in terms of stress-strain relationship are given as

$$\begin{bmatrix} \sigma_{xx\delta}(x,z) \\ \sigma_{zz\delta}(x,z) \\ \sigma_{xz\delta}(x,z) \end{bmatrix} = \begin{bmatrix} C_{11\delta}(\Phi) & C_{12\delta}(\Phi) & C_{16\delta}(\Phi) \\ C_{12\delta}(\Phi) & C_{22\delta}(\Phi) & C_{26\delta}(\Phi) \\ C_{16\delta}(\Phi) & C_{26\delta}(\Phi) & C_{66\delta}(\Phi) \end{bmatrix} \begin{bmatrix} \varepsilon_{xx\delta}(x,z) - \varepsilon_{xx0\delta}(\Phi) \\ \varepsilon_{zz\delta}(x,z) - \varepsilon_{zz0\delta}(\Phi) \\ 2\varepsilon_{xz\delta}(x,z) - 2\varepsilon_{xz0\delta}(\Phi) \end{bmatrix}, \quad (\delta = w,\ f,\ M), \tag{1}$$

where $\sigma_{xx\delta}(x,z)$, $\sigma_{zz\delta}(x,z)$, $\sigma_{xz\delta}(x,z)$ are the stress components, $\varepsilon_{xx\delta}(x,z)$, $\varepsilon_{zz\delta}(x,z)$, $\varepsilon_{xz\delta}(x,z)$ are the strain components, $C_{11\delta}(\Phi)$, $C_{12\delta}(\Phi)$, ..., $C_{66\delta}(\Phi)$ are the components of the stiffness matrix and $\varepsilon_{xx0\delta}(\Phi)$, $\varepsilon_{zz0\delta}(\Phi)$, $\varepsilon_{xz0\delta}(\Phi)$ ($\delta = w,\ f,\ M$) are the initial strain components. The subscripts w and f refer to the warp and fill fiber bundles, respectively. The initial strain components are given in Appendix A.

Due to symmetry conditions, we consider only the region $0 \le x \le 5l/2$, $0 \le z \le 2Nh$. Let $u_{i\delta}(x,z)$ ($i = x,\ z,\ \delta = w,\ f,\ M$) be the displacement components. The boundary conditions at $x = 0$ for the kth lamina ($1 \le k \le N$) occupying the region $0 \le x \le 5l/2$, $2(k\text{-}1)h \le z \le 2kh$ may be stated as follows:

Case 1

Odd number of k ($k = 1, 3, 5, ...$)

$$\left.\begin{array}{rcll} \sigma_{xxf}(0,z) & = & 0, & 2(k-1)h \le z < 2(k-1)h + a, \\ u_{xf}(0,z) & = & 0, & 2(k-1)h + a \le z \le (2k-1)h, \\ u_{xw}(0,z) & = & 0, & (2k-1)h \le z \le 2kh, \end{array}\right\} \tag{2}$$

$$\left.\begin{array}{rcll} \sigma_{xzf}(0,z) & = & 0, & 2(k-1)h \le z \le (2k-1)h, \\ \sigma_{xzw}(0,z) & = & 0, & (2k-1)h \le z \le 2kh, \end{array}\right\} \tag{3}$$

Even number of k ($k = 2, 4, 6, ...$)

$$\left.\begin{array}{rcll} u_{xw}(0,z) & = & 0, & 2(k-1)h \le z \le (2k-1)h, \\ u_{xf}(0,z) & = & 0, & (2k-1)h \le z \le 2kh - a, \\ \sigma_{xxf}(0,z) & = & 0, & 2kh - a < z \le 2kh, \end{array}\right\} \tag{4}$$

$$\left.\begin{array}{rcll} \sigma_{xzw}(0,z) & = & 0, & 2(k-1)h \le z \le (2k-1)h, \\ \sigma_{xzf}(0,z) & = & 0, & (2k-1)h \le z \le 2kh, \end{array}\right\} \tag{5}$$

Case 2

Odd number of k ($k = 1, 3, 5, ...$)

$$\left.\begin{array}{rcll} u_{xw}(0,z) & = & 0, & 2(k-1)h \le z \le (2k-1)h, \\ u_{xf}(0,z) & = & 0, & (2k-1)h \le z \le 2kh - a, \\ \sigma_{xxf}(0,z) & = & 0, & 2kh - a < z \le 2kh, \end{array}\right\} \tag{6}$$

$$\left.\begin{array}{rcll} \sigma_{xzw}(0,z) & = & 0, & 2(k-1)h \le z \le (2k-1)h, \\ \sigma_{xzf}(0,z) & = & 0, & (2k-1)h \le z \le 2kh, \end{array}\right\} \tag{7}$$

Even number of k ($k = 2, 4, 6, ...$)

$$\left.\begin{array}{rcll} \sigma_{xxf}(0,z) & = & 0, & 2(k-1)h \le z < 2(k-1)h + a, \\ u_{xf}(0,z) & = & 0, & 2(k-1)h + a \le z \le (2k-1)h, \\ u_{xw}(0,z) & = & 0, & (2k-1)h \le z \le 2kh, \end{array}\right\} \tag{8}$$

$$\left.\begin{array}{rcll} \sigma_{xzf}(0,z) & = & 0, & 2(k-1)h \le z \le (2k-1)h, \\ \sigma_{xzw}(0,z) & = & 0, & (2k-1)h \le z \le 2kh. \end{array}\right\} \tag{9}$$

The loading conditions are as follows:

Case 1

Odd number of k ($k = 1, 3, 5, ...$)

$$\left.\begin{array}{rcll} u_{xw}(5l/2,z) & = & u_x^*, & 2(k-1)h \le z \le (2k-1)h, \\ u_{xM}(5l/2,z) & = & u_x^*, & (2k-1)h \le z \le 2kh, \end{array}\right\} \tag{10}$$

Even number of k ($k = 2, 4, 6, ...$)

$$\left.\begin{array}{rcll} u_{xM}(5l/2,z) & = & u_x^*, & 2(k-1)h \le z \le (2k-1)h, \\ u_{xw}(5l/2,z) & = & u_x^*, & (2k-1)h \le z \le 2kh, \end{array}\right\} \tag{11}$$

Case 2

Odd number of k ($k = 1, 3, 5, ...$)

$$\left.\begin{array}{rcll} u_{xM}(5l/2,z) & = & u_x^*, & 2(k-1)h \le z \le (2k-1)h, \\ u_{xw}(5l/2,z) & = & u_x^*, & (2k-1)h \le z \le 2kh, \end{array}\right\} \tag{12}$$

Even number of k ($k = 2, 4, 6, ...$)

$$\left.\begin{array}{rcll} u_{xw}(5l/2,z) & = & u_x^*, & 2(k-1)h \le z \le (2k-1)h, \\ u_{xM}(5l/2,z) & = & u_x^*, & (2k-1)h \le z \le 2kh, \end{array}\right\} \tag{13}$$

where u_x^* is the uniform displacement in the x-direction induced by the mechanical and thermal loads. For the case of the woven laminates with an infinite number of layers ($N = \infty$), we only need to consider the repeating unit defined by $0 \le x \le 5l/2$, $0 \le z \le 2h$ and symmetry conditions are imposed on the top surface of the repeating unit ($z = 2h$).

The loading case considered in this study is dominated by the opening mode of deformation (Mode I). Therefore, only the Mode I stress intensity factors K_{I} are studied. The definitions of the stress intensity factors K_{I} at the tips of the fill fiber bundle cracks give

Case 1

Odd number of k ($k = 1, 3, 5, ...$)

$$K_{\mathrm{I}} = \begin{cases} \lim\limits_{z\to\{2(k-1)h+a\}^{+}} \left[2\pi\left\{z-2(k-1)h-a\right\}\right]^{1/2}\sigma_{xxf}(0,z), & (a<h), \\ \lim\limits_{z\to\{(2k-1)h\}^{+}} (2\pi)^{1/2}\left\{z-(2k-1)h\right\}^{\omega}\sigma_{xxw}(0,z), & (a=h), \end{cases} \tag{14}$$

Even number of k ($k = 2, 4, 6, ...$)

$$K_{\mathrm{I}} = \begin{cases} \lim\limits_{z\to(2kh-a)^{-}} \left\{2\pi(2kh-a-z)\right\}^{1/2}\sigma_{xxf}(0,z), & (a<h), \\ \lim\limits_{z\to\{(2k-1)h\}^{-}} (2\pi)^{1/2}\left\{(2k-1)h-z\right\}^{\omega}\sigma_{xxw}(0,z), & (a=h), \end{cases} \tag{15}$$

Case 2

Odd number of k ($k = 1, 3, 5, ...$)

$$K_{\mathrm{I}} = \begin{cases} \lim\limits_{z\to(2kh-a)^{-}} \left\{2\pi(2kh-a-z)\right\}^{1/2}\sigma_{xxf}(0,z), & (a<h), \\ \lim\limits_{z\to\{(2k-1)h\}^{-}} (2\pi)^{1/2}\left\{(2k-1)h-z\right\}^{\omega}\sigma_{xxw}(0,z), & (a=h), \end{cases} \tag{16}$$

Even number of k ($k = 2, 4, 6, ...$)

$$K_{\mathrm{I}} = \begin{cases} \lim\limits_{z\to\{2(k-1)h+a\}^{+}} \left[2\pi\left\{z-2(k-1)h-a\right\}\right]^{1/2}\sigma_{xxf}(0,z), & (a<h), \\ \lim\limits_{z\to\{(2k-1)h\}^{+}} (2\pi)^{1/2}\left\{z-(2k-1)h\right\}^{\omega}\sigma_{xxw}(0,z), & (a=h), \end{cases} \tag{17}$$

where ω is the order of stress singularity at the interface tip of the crack, and the ω values can be determined using the analytical method [10] (Appendix B). Using the crack opening displacement, Eqs. (14)−(17) can be rewritten as

Case 1

Odd number of k ($k = 1, 3, 5, ...$)

$$K_{\mathrm{I}} = \begin{cases} (2\pi)^{1/2}\mu^{*}\left\{2(k-1)h+a-z\right\}^{-1/2}u_{xf}(0,z), & (a<h), \\ (2\pi)^{1/2}\mu^{*}\left\{(2k-1)h-z\right\}^{-(1-\omega)}u_{xf}(0,z), & (a=h), \\ & (2(k-1)h \le z < 2(k-1)h+a), \end{cases} \tag{18}$$

Even number of k ($k = 2, 4, 6, ...$)

$$K_{\mathrm{I}} = \begin{cases} (2\pi)^{1/2}\mu^{*}(z-2kh+a)^{-1/2}u_{xf}(0,z), & (a<h), \\ (2\pi)^{1/2}\mu^{*}\left\{z-(2k-1)h\right\}^{-(1-\omega)}u_{xf}(0,z), & (a=h), \\ & (2kh-a < z \le 2kh), \end{cases} \tag{19}$$

Case 2

Odd number of k ($k = 1, 3, 5, ...$)

$$K_{\mathrm{I}} = \begin{cases} (2\pi)^{1/2}\mu^*(z-2kh+a)^{-1/2}u_{xf}(0,z), & (a<h), \\ (2\pi)^{1/2}\mu^*\left\{z-(2k-1)h\right\}^{-(1-\omega)}u_{xf}(0,z), & (a=h), \\ & (2kh-a<z\leq 2kh), \end{cases} \tag{20}$$

Even number of k ($k = 2, 4, 6, ...$)

$$K_{\mathrm{I}} = \begin{cases} (2\pi)^{1/2}\mu^*\left\{2(k-1)h+a-z\right\}^{-1/2}u_{xf}(0,z), & (a<h), \\ (2\pi)^{1/2}\mu^*\left\{(2k-1)h-z\right\}^{-(1-\omega)}u_{xf}(0,z), & (a=h), \\ & (2(k-1)h\leq z<2(k-1)h+a), \end{cases} \tag{21}$$

where μ^* is the constant (see Appendix C).

Highly accurate stress intensity factors can be obtained by placing special singular elements around the crack tip. The singular triangle element constructed by Stern [11] is used to obtain the proper displacement field near the interface tip of the crack. The surrounding nonsingular elements are six- and eight-node isoparametric elements.

5 Numerical Results and Discussion

The woven geometry of the 5HS woven laminates is determined by the parameters $l = 4h/3\tan\theta$ and $d = l/8$. From the geometrical parameters of the actual T800H/3633 5HS woven laminates, the undulation angle is estimated to be $\theta = 9.0$ deg. The value of a fiber volume fraction in the fiber bundles V_F^B is taken as 0.85, corresponding to that of actual T800H/3633 5HS woven laminates. The fuel tanks in the space vehicles contain cryogen such as liquid hydrogen or oxygen, at very low temperatures like 20 K for liquid hydrogen, and, hence, the temperature $\Phi = 20$ K is considered. The stress-free temperature Φ_s is assumed to be 453 K [12]. The finite element code was verified by comparing the results for the stress intensity factors of transverse cracks in unidirectional glass fiber reinforced polymer composite laminates with the theoretical results [13].

Figure 2 shows the normalized stress intensity factors K_{I}/K_0 of the cracks in the first layer ($k = 1$, $N = 1, 2, \infty$) under pure thermal load (i.e. $\sigma_{xx}^* = 0$ MPa) at 20 K as a function of crack length to fiber bundle thickness ratio a/h for Case 1. The stress intensity factor results are normalized by $K_0 = E_{xf}(\Phi_s)\alpha_{xf}(\Phi_s)\Phi_s(\pi h)^{1/2}$. The thermally induced stress intensity factors in the first layer increase with the increase in N. The stress intensity factors first increase, reach a peak and then finally decrease with increasing a/h. This characteristic behavior occurs because the warp fiber bundles are significantly stiffer in the

loading direction than the fill fiber bundles, and this feature leads to a crack arrest. Also, the positions of the peaks in the stress intensity factors for $N = 1, 2, \infty$ are different. This implies that the interaction with adjoining layers influences the crack behavior. Figure 3 depicts the corresponding results for

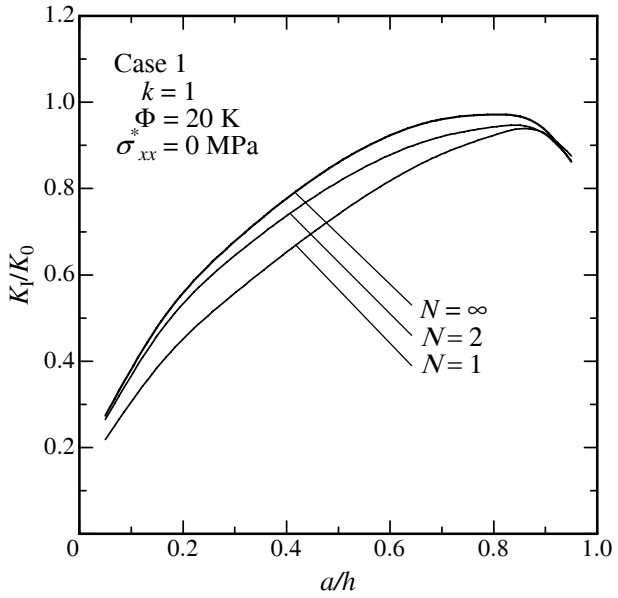

Figure 2 Normalized stress intensity factors K_{I}/K_0 vs. crack length to fiber bundle thickness ratio a/h for $k = 1$ under $\sigma^*_{xx} = 0$ MPa at 20 K (Case 1).

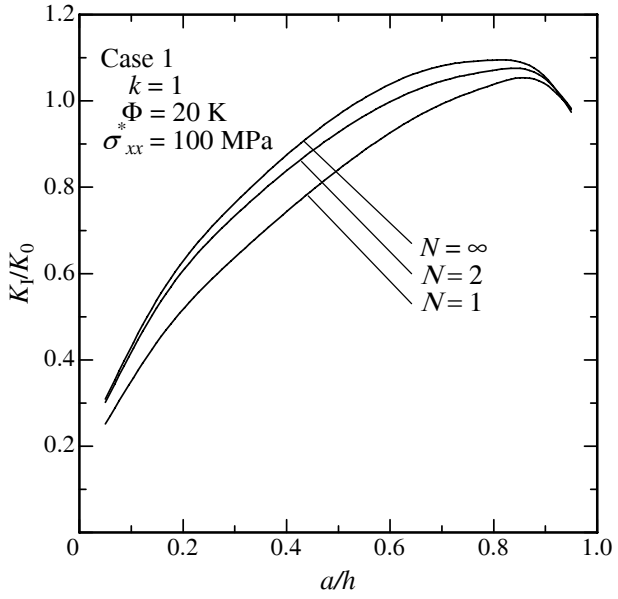

Figure 3 Normalized stress intensity factors K_{I}/K_0 vs. crack length to fiber bundle thickness ratio a/h for $k = 1$ under $\sigma^*_{xx} = 100$ MPa at 20 K (Case 1).

the normalized stress intensity factors $K_{\rm I}/K_0$ under mechanical load (i.e. $\sigma^*_{xx} =$ 100 MPa) at 20 K. It is found that the stress intensity factors under combined mechanical and thermal loads are larger than those under pure thermal load. The dependence of the stress intensity factors on the crack length becomes large, when the woven laminates are subjected to combined loads. Figure 4 contains plots of the normalized stress intensity factors $K_{\rm I}/K_0$ of the cracks in the first layer ($k = 1$, $N = 1$, 2, ∞) under mechanical load at 20 K against a/h for Case 2. The stress intensity factors initially increase and then decrease as a/h increases in the same fashion as those for Case 1. For Case 2, the stress intensity factors for $N = 1$ are larger than those for $N = 2$, ∞. Also, the values of the stress intensity factors for Case 2 and $N = 1$ are higher than those for Case 1 and $N = 1$, 2, ∞. These reveal that the edge cracks play an important role in the fracture behavior of woven composites. In Figure 5 the normalized stress intensity factors $K_{\rm I}/K_0$ of the cracks in the surface layer ($k = N$, $N =$ 1, 2) under mechanical load at 20 K are plotted as a function of a/h for Cases 1 and 2. The numerical results for the stress intensity factors of the cracks in the surface layer exhibit similar trends for the stress intensity factor variation with a/h to those of the cracks in the first layer. The stress intensity factors of the internal and edge cracks for $N = 2$ are larger than those for $N = 1$. Also, the stress intensity factors of the edge cracks are larger than those of the internal cracks. Therefore, as noted above, it is important to understand the edge crack behavior in the woven composite laminates. This result is in accord

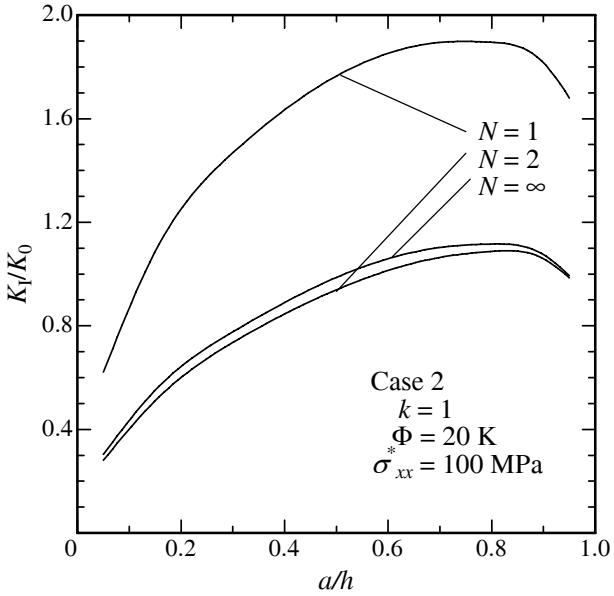

Figure 4 Normalized stress intensity factors $K_{\rm I}/K_0$ vs. crack length to fiber bundle thickness ratio a/h for $k = 1$ under $\sigma^*_{xx} = 100$ MPa at 20 K (Case 2).

with the experimental observations on damage development mechanisms in T800H/3633 5HS woven laminates at cryogenic temperatures [14].

The normalized stress intensity factors K_{I}/K_0' at the crack tip located at the warp/fill interface ($a/h = 1.0$) in the first layer ($k = 1$, $N = 1, 2, \infty$) are listed in Table 2 for Cases 1 and 2 under $\sigma_{xx}^* = 0$, 100 MPa at 20 K. The stress intensity factors are normalized by $K_0' = E_{xf}(\Phi_s)\alpha_{xf}(\Phi_s)\Phi_s\pi^{1/2}h^{\omega}$. The order of stress singularity ω at the tip of a crack located at the warp/fill interface is 0.3681. Except for the edge crack (Case 2, $N = 1$), the stress intensity factors increase as increasing N. The values of the normalized stress intensity factors

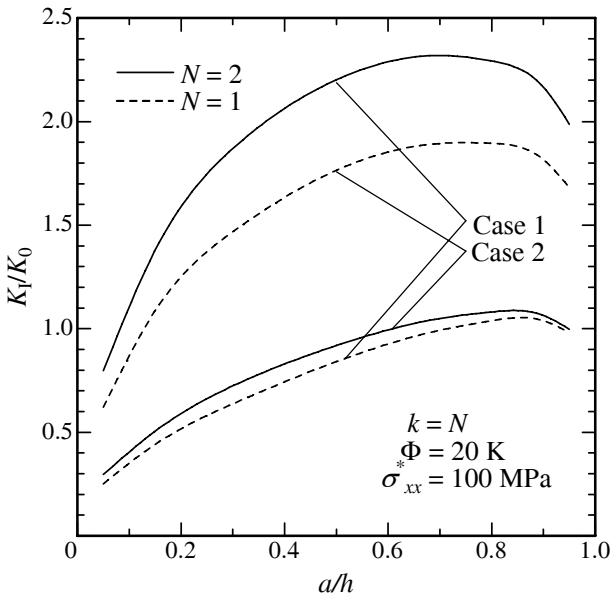

Figure 5 Normalized stress intensity factors K_{I}/K_0 vs. crack length to fiber bundle thickness ratio a/h for $k = N$ under $\sigma_{xx}^* = 100$ MPa at 20 K (Cases 1 and 2).

Table 2 Normalized stress intensity factors K_{I}/K_0' for $k = 1$ under $\sigma_{xx}^* = 0$, 100 MPa at 20 K (Cases 1 and 2)

N			1	2	∞
K_{I}/K_0'	Case 1	$\sigma_{xx}^* =$ 0 MPa	2.362	2.404	4.786
		$\sigma_{xx}^* =$ 100 MPa	3.091	3.143	5.603
	Case 2	$\sigma_{xx}^* =$ 0 MPa	4.630	2.292	4.786
		$\sigma_{xx}^* =$ 100 MPa	5.520	2.956	5.603

Table 3 Normalized stress intensity factors K_{I}/K_0' for $k = N$ under $\sigma_{xx}^* = 0$, 100 MPa at 20 K (Cases 1 and 2)

N			1	2
K_{I}/K_0'	Case 1	$\sigma_{xx}^* =$ 0 MPa	2.362	5.146
		$\sigma_{xx}^* =$ 100 MPa	3.091	5.995
	Case 2	$\sigma_{xx}^* =$ 0 MPa	4.630	2.479
		$\sigma_{xx}^* =$ 100 MPa	5.520	3.194

K_{I}/K_0' at the interface tip of the crack in the surface layer ($k = N$, $N = 1$, 2) are tabulated in Table 3 for Cases 1 and 2 under $\sigma_{xx}^* = 0$, 100 MPa at 20 K. For the same value of N, it is clear that the stress intensity factors of the edge cracks are larger than those of the internal cracks. For both the internal and edge cracks, the stress intensity factors for $N = 2$ are larger than those for $N = 1$.

6 Conclusions

The cryogenic singular stresses at the crack tip in multi-layer woven CFRP composite laminates with temperature-dependent material properties under tension are examined by using a finite element method. The stress intensity factors depend on the crack type and the number of layers, and the crack arrest may occur when the cracks approach the interfaces between two orthogonal fiber bundles. Also, the edge cracks are important in the cryogenic fracture behavior of the woven laminates. The present results are expected to offer a basic understanding of the cryogenic fracture behavior of woven laminates which will be used in cryogenic storage systems.

ACKNOWLEDGEMENTS.

The work was supported by the Research Fellowships of the Japan Society for the Promotion of Science for Young Scientists.

Appendix A

The initial strain components $\varepsilon_{xx0\delta}(\Phi)$, $\varepsilon_{zz0\delta}(\Phi)$, $\varepsilon_{xz0\delta}(\Phi)$ ($\delta = w,\ f,\ M$) involved in Eq. (1) are given by

$$\begin{bmatrix} \varepsilon_{xx0\delta}(\Phi) \\ \varepsilon_{zz0\delta}(\Phi) \\ 2\varepsilon_{xz0\delta}(\Phi) \end{bmatrix} =$$

$$\begin{cases} \left[\ T\ \right]^{-1} \begin{bmatrix} \varepsilon^T_{LLw}(\Phi) - \dfrac{E_{Tw}(\Phi)}{E_{Lw}(\Phi)}\nu_{LTw}(\Phi)\{\varepsilon_{yy0}(\Phi) - \varepsilon^T_{TTw}(\Phi)\} \\ \varepsilon^T_{TTw}(\Phi) - \nu_{TTw}(\Phi)\{\varepsilon_{yy0}(\Phi) - \varepsilon^T_{TTw}(\Phi)\} \\ 0 \end{bmatrix}, \\ \qquad\qquad (\delta = w), \\ \begin{bmatrix} \varepsilon^T_{xxf}(\Phi) - \dfrac{E_{yf}(\Phi)}{E_{xf}(\Phi)}\nu_{xyf}(\Phi)\{\varepsilon_{yy0}(\Phi) - \varepsilon^T_{yyf}(\Phi)\} \\ \varepsilon^T_{zzf}(\Phi) - \nu_{yzf}(\Phi)\{\varepsilon_{yy0}(\Phi) - \varepsilon^T_{yyf}(\Phi)\} \\ 0 \end{bmatrix}, \\ \qquad\qquad (\delta = f), \\ \begin{bmatrix} \varepsilon^T_{M}(\Phi) - \nu_{M}(\Phi)\{\varepsilon_{yy0}(\Phi) - \varepsilon^T_{M}(\Phi)\} \\ \varepsilon^T_{M}(\Phi) - \nu_{M}(\Phi)\{\varepsilon_{yy0}(\Phi) - \varepsilon^T_{M}(\Phi)\} \\ 0 \end{bmatrix}, \\ \qquad\qquad (\delta = M), \end{cases} \tag{A.1}$$

where the superscript -1 represents the matrix inverse and $[T]$ is a transformation matrix given by

$$\left[\ T\ \right] = \begin{bmatrix} \cos^2\theta & \sin^2\theta & \cos\theta\sin\theta \\ \sin^2\theta & \cos^2\theta & -\cos\theta\sin\theta \\ -2\cos\theta\sin\theta & 2\cos\theta\sin\theta & \cos^2\theta - \sin^2\theta \end{bmatrix}. \tag{A.2}$$

The elastic properties of the warp fiber bundles $E_{Lw}(\Phi)$, $E_{Tw}(\Phi)$, $\nu_{LTw}(\Phi)$, $\nu_{TTw}(\Phi)$ and fill fiber bundles $E_{xf}(\Phi)$, $E_{yf}(\Phi)$, $\nu_{xyf}(\Phi)$, $\nu_{yzf}(\Phi)$ are given as

$$\left.\begin{aligned}
&E_{Lw}(\Phi) = E_{yf}(\Phi) = E_L^B(\Phi),\\
&E_{Tw}(\Phi) = E_{xf}(\Phi) = E_T^B(\Phi),\\
&\nu_{LTw}(\Phi) = \nu_{yzf}(\Phi) = \nu_{LT}^B(\Phi),\\
&\nu_{TTw}(\Phi) = \nu_{TT}^B(\Phi) = \frac{E_T^B(\Phi) - 2G_{TT}^B(\Phi)}{2G_{TT}^B(\Phi)},\\
&\nu_{xyf}(\Phi) = \nu_{TL}^B(\Phi) = \frac{E_T^B(\Phi)}{E_L^B(\Phi)}\nu_{LT}^B(\Phi),
\end{aligned}\right\} \tag{A.3}$$

where the subscripts x, y and z denote the three axes of the Cartesian coordinate system. The thermal strains $\varepsilon_{LLw}^T(\Phi)$, $\varepsilon_{TTw}^T(\Phi)$, $\varepsilon_{xxf}^T(\Phi) = \varepsilon_{zzf}^T(\Phi)$, $\varepsilon_{yyf}^T(\Phi)$, $\varepsilon_M^T(\Phi)$ are

$$\left.\begin{aligned}
\varepsilon_{LLw}^T(\Phi) &= \int_{\Phi_s}^{\Phi} \alpha_L^B(\phi)d\phi,\\
\varepsilon_{TTw}^T(\Phi) &= \int_{\Phi_s}^{\Phi} \alpha_T^B(\phi)d\phi,\\
\varepsilon_{xxf}^T(\Phi) &= \varepsilon_{zzf}^T(\Phi)\\
&= \int_{\Phi_s}^{\Phi} \alpha_T^B(\phi)d\phi,\\
\varepsilon_{yyf}^T(\Phi) &= \int_{\Phi_s}^{\Phi} \alpha_L^B(\phi)d\phi,\\
\varepsilon_M^T(\Phi) &= \int_{\Phi_s}^{\Phi} \alpha_M(\phi)d\phi.
\end{aligned}\right\} \tag{A.4}$$

The uniform strain (i.e. constant in the x-z plane) in the y-direction $\varepsilon_{yy0}(\Phi)$ can be found from the condition:

$$\frac{\iint_{\Omega_w} \sigma_{yyw}(x,z)dxdz + \iint_{\Omega_f} \sigma_{yyf}(x,z)dxdz + \iint_{\Omega_M} \sigma_{yyM}(x,z)dxdz}{\Omega_w + \Omega_f + \Omega_M} = 0, \tag{A.5}$$

where Ω_δ ($\delta = w,\ f,\ M$) denote the regions of the warp fiber bundles, fill fiber bundles and matrix, respectively. The stresses $\sigma_{yy\delta}(x,z)$ ($\delta = w,\ f,\ M$) can be written as:

$$\sigma_{yy\delta}(x,z) = \begin{cases} E_{Tw}(\Phi)\{\varepsilon_{yy0}(\Phi) - \varepsilon^T_{TTw}(\Phi)\} + \dfrac{E_{Tw}(\Phi)}{E_{Lw}(\Phi)}\nu_{LTw}(\Phi)\sigma_{LLw}(x,z) \\ \quad +\nu_{TTw}(\Phi)\sigma_{TTw}(x,z), & (\delta = w), \\ E_{yf}(\Phi)\{\varepsilon_{yy0}(\Phi) - \varepsilon^T_{yyf}(\Phi)\} + \dfrac{E_{yf}(\Phi)}{E_{xf}(\Phi)}\nu_{xyf}(\Phi)\sigma_{xxf}(x,z) \\ \quad +\nu_{yzf}(\Phi)\sigma_{zzf}(x,z), & (\delta = f), \\ E_M(\Phi)\{\varepsilon_{yy0}(\Phi) - \varepsilon^T_M(\Phi)\} \\ \quad +\nu_M(\Phi)\{\sigma_{xxM}(x,z) + \sigma_{zzM}(x,z)\}, & (\delta = M), \end{cases} \tag{A.6}$$

where $\sigma_{LLw}(x,z)$ and $\sigma_{TTw}(x,z)$ are given by:

$$\begin{bmatrix} \sigma_{LLw}(x,z) \\ \sigma_{TTw}(x,z) \end{bmatrix} = \begin{bmatrix} \cos^2\theta & \sin^2\theta & 2\cos\theta\sin\theta \\ \sin^2\theta & \cos^2\theta & -2\cos\theta\sin\theta \end{bmatrix} \begin{bmatrix} \sigma_{xxw}(x,z) \\ \sigma_{zzw}(x,z) \\ \sigma_{xzw}(x,z) \end{bmatrix}. \tag{A.7}$$

Appendix B

The order of stress singularity at the interface tip of the crack is determined by the roots of the following equation:

$$|\boldsymbol{\Delta}(\omega)| = 0, \tag{B.1}$$

where $\boldsymbol{\Delta}(\omega)$ is an 8×8 square matrix and $|\boldsymbol{\Delta}(\omega)|$ is the determinant of the square matrix $\boldsymbol{\Delta}(\omega)$. The 8×8 matrix $\boldsymbol{\Delta}(\omega)$ is given by

$$\boldsymbol{\Delta}(\omega) =$$

$$\begin{bmatrix} \Delta_{1,1}(\omega) & \Delta_{1,2}(\omega) & \Delta_{1,3}(\omega) & \Delta_{1,4}(\omega) & 0 & 0 & 0 & 0 \\ \Delta_{2,1}(\omega) & \Delta_{2,2}(\omega) & \Delta_{2,3}(\omega) & \Delta_{2,4}(\omega) & 0 & 0 & 0 & 0 \\ \Delta_{3,1}(\omega) & \Delta_{3,2}(\omega) & \Delta_{3,3}(\omega) & \Delta_{3,4}(\omega) & 0 & 0 & 0 & 0 \\ \Delta_{4,1}(\omega) & \Delta_{4,2}(\omega) & \Delta_{4,3}(\omega) & \Delta_{4,4}(\omega) & 0 & 0 & 0 & 0 \\ \Delta_{5,1}(\omega) & \Delta_{5,2}(\omega) & \Delta_{5,3}(\omega) & \Delta_{5,4}(\omega) & \Delta_{5,5}(\omega) & \Delta_{5,6}(\omega) & \Delta_{5,7}(\omega) & \Delta_{5,8}(\omega) \\ \Delta_{6,1}(\omega) & \Delta_{6,2}(\omega) & \Delta_{6,3}(\omega) & \Delta_{6,4}(\omega) & \Delta_{6,5}(\omega) & \Delta_{6,6}(\omega) & \Delta_{6,7}(\omega) & \Delta_{6,8}(\omega) \\ \Delta_{7,1}(\omega) & \Delta_{7,2}(\omega) & \Delta_{7,3}(\omega) & \Delta_{7,4}(\omega) & \Delta_{7,5}(\omega) & \Delta_{7,6}(\omega) & \Delta_{7,7}(\omega) & \Delta_{7,8}(\omega) \\ \Delta_{8,1}(\omega) & \Delta_{8,2}(\omega) & \Delta_{8,3}(\omega) & \Delta_{8,4}(\omega) & \Delta_{8,5}(\omega) & \Delta_{8,6}(\omega) & \Delta_{8,7}(\omega) & \Delta_{8,8}(\omega) \end{bmatrix}, \tag{B.2}$$

in which

$$
\begin{aligned}
&\Delta_{1,1}(\omega) = \lambda_{xf1}\,(-1)^{-\omega}, && \Delta_{1,2}(\omega) = \overline{\lambda}_{xf1}\,(-1)^{-\omega},\\
&\Delta_{1,3}(\omega) = \lambda_{xf2}\,(-1)^{-\omega}, && \Delta_{1,4}(\omega) = \overline{\lambda}_{xf2}\,(-1)^{-\omega},\\
&\Delta_{2,1}(\omega) = \lambda_{xzf1}\,(-1)^{-\omega}, && \Delta_{2,2}(\omega) = \overline{\lambda}_{xzf1}\,(-1)^{-\omega},\\
&\Delta_{2,3}(\omega) = \lambda_{xzf2}\,(-1)^{-\omega}, && \Delta_{2,4}(\omega) = \overline{\lambda}_{xzf2}\,(-1)^{-\omega},\\
&\Delta_{3,1}(\omega) = \lambda_{xzw1}, && \Delta_{3,2}(\omega) = \overline{\lambda}_{xzw1},\\
&\Delta_{3,3}(\omega) = \lambda_{xzw2}, && \Delta_{3,4}(\omega) = \overline{\lambda}_{xzw2},\\
&\Delta_{4,1}(\omega) = \eta_{xw1}, && \Delta_{4,2}(\omega) = \overline{\eta}_{xw1},\\
&\Delta_{4,3}(\omega) = \eta_{xw2}, && \Delta_{4,4}(\omega) = \overline{\eta}_{xw2},\\
&\Delta_{5,1}(\omega) = \lambda_{zf1}\,(\zeta_{f1})^{-\omega}, && \Delta_{5,2}(\omega) = \overline{\lambda}_{zf1}\,(\overline{\zeta}_{f1})^{-\omega},\\
&\Delta_{5,3}(\omega) = \lambda_{zf2}\,(\zeta_{f2})^{-\omega}, && \Delta_{5,4}(\omega) = \overline{\lambda}_{zf2}\,(\overline{\zeta}_{f2})^{-\omega},\\
&\Delta_{5,5}(\omega) = -\lambda_{zw1}\,(\zeta_{w1})^{-\omega}, && \Delta_{5,6}(\omega) = -\overline{\lambda}_{zw1}\,(\overline{\zeta}_{w1})^{-\omega},\\
&\Delta_{5,7}(\omega) = -\lambda_{zw2}\,(\zeta_{w2})^{-\omega}, && \Delta_{5,8}(\omega) = -\overline{\lambda}_{zw2}\,(\overline{\zeta}_{w2})^{-\omega},\\
&\Delta_{6,1}(\omega) = \lambda_{xzf1}\,(\zeta_{f1})^{-\omega}, && \Delta_{6,2}(\omega) = \overline{\lambda}_{xzf1}\,(\overline{\zeta}_{f1})^{-\omega},\\
&\Delta_{6,3}(\omega) = \lambda_{xzf2}\,(\zeta_{f2})^{-\omega}, && \Delta_{6,4}(\omega) = \overline{\lambda}_{xzf2}\,(\overline{\zeta}_{f2})^{-\omega},\\
&\Delta_{6,5}(\omega) = -\lambda_{xzw1}\,(\zeta_{w1})^{-\omega}, && \Delta_{6,6}(\omega) = -\overline{\lambda}_{xzw1}\,(\overline{\zeta}_{w1})^{-\omega},\\
&\Delta_{6,7}(\omega) = -\lambda_{xzw2}\,(\zeta_{w2})^{-\omega}, && \Delta_{6,8}(\omega) = -\overline{\lambda}_{xzw2}\,(\overline{\zeta}_{w2})^{-\omega},\\
&\Delta_{7,1}(\omega) = \eta_{zf1}\,(\zeta_{f1})^{1-\omega}, && \Delta_{7,2}(\omega) = \overline{\eta}_{zf1}\,(\overline{\zeta}_{f1})^{1-\omega},\\
&\Delta_{7,3}(\omega) = \eta_{zf2}\,(\zeta_{f2})^{1-\omega}, && \Delta_{7,4}(\omega) = \overline{\eta}_{zf2}\,(\overline{\zeta}_{f2})^{1-\omega},\\
&\Delta_{7,5}(\omega) = -\eta_{zw1}\,(\zeta_{w1})^{1-\omega}, && \Delta_{7,6}(\omega) = -\overline{\eta}_{zw1}\,(\overline{\zeta}_{w1})^{1-\omega},\\
&\Delta_{7,7}(\omega) = -\eta_{zw2}\,(\zeta_{w2})^{1-\omega}, && \Delta_{7,8}(\omega) = -\overline{\eta}_{zw2}\,(\overline{\zeta}_{w2})^{1-\omega},\\
&\Delta_{8,1}(\omega) = \eta_{xf1}\,(\zeta_{f1})^{1-\omega}, && \Delta_{8,2}(\omega) = \overline{\eta}_{xf1}\,(\overline{\zeta}_{f1})^{1-\omega},\\
&\Delta_{8,3}(\omega) = \eta_{xf2}\,(\zeta_{f2})^{1-\omega}, && \Delta_{8,4}(\omega) = \overline{\eta}_{xf2}\,(\overline{\zeta}_{f2})^{1-\omega},\\
&\Delta_{8,5}(\omega) = -\eta_{xw1}\,(\zeta_{w1})^{1-\omega}, && \Delta_{8,6}(\omega) = -\overline{\eta}_{xw1}\,(\overline{\zeta}_{w1})^{1-\omega},\\
&\Delta_{8,7}(\omega) = -\eta_{xw2}\,(\zeta_{w2})^{1-\omega}, && \Delta_{8,8}(\omega) = -\overline{\eta}_{xw2}\,(\overline{\zeta}_{w2})^{1-\omega}.
\end{aligned}
\tag{B.3}
$$

In Eq. (B.3), the overbar represents the complex conjugate and $\lambda_{x\delta' j}$, $\lambda_{z\delta' j}$, $\lambda_{xz\delta' j}$ $(\delta' = w,\ f;\ j = 1,\ 2)$ are given by

$$
\left.
\begin{aligned}
&\lambda_{x\delta' j} = C_{12\delta'}(\Phi)\eta_{z\delta' j} + C_{11\delta'}(\Phi)\zeta_{\delta' j}\,\eta_{x\delta' j},\\
&\lambda_{z\delta' j} = C_{22\delta'}(\Phi)\eta_{z\delta' j} + C_{12\delta'}(\Phi)\zeta_{\delta' j}\,\eta_{x\delta' j},\\
&\lambda_{xz\delta' j} = C_{66\delta'}(\Phi)(\zeta_{\delta' j}\,\eta_{z\delta' j} + \eta_{x\delta' j}),
\end{aligned}
\right\}
(\delta' = w,\ f;\ j = 1,\ 2). \tag{B.4}
$$

$\zeta^2_{\delta' j}$ $(\delta' = w,\ f;\ j = 1,\ 2)$ are the roots of the following equation:

$$
\begin{vmatrix}
C_{22\delta'}(\Phi) + C_{66\delta'}(\Phi)\zeta^2_{\delta'} & \left\{C_{12\delta'}(\Phi) + C_{66\delta'}(\Phi)\right\}\zeta_{\delta'}\\
\left\{C_{12\delta'}(\Phi) + C_{66\delta'}(\Phi)\right\}\zeta_{\delta'} & C_{66\delta'}(\Phi) + C_{11\delta'}(\Phi)\zeta^2_{\delta'}
\end{vmatrix} = 0, \quad (\delta' = w,\ f). \tag{B.5}
$$

Values of $\eta_{x\delta' j}$, $\eta_{z\delta' j}$ ($\delta' = w,\ f;\ j = 1,\ 2$) can be found, satisfying the following equation:

$$\begin{bmatrix} C_{22\delta'}(\Phi) + C_{66\delta'}(\Phi)\zeta_{\delta' j}^2 & \{C_{12\delta'}(\Phi) + C_{66\delta'}(\Phi)\}\,\zeta_{\delta' j} \\ \{C_{12\delta'}(\Phi) + C_{66\delta'}(\Phi)\}\,\zeta_{\delta' j} & C_{66\delta'}(\Phi) + C_{11\delta'}(\Phi)\zeta_{\delta' j}^2 \end{bmatrix} \begin{bmatrix} \eta_{x\delta' j} \\ \eta_{z\delta' j} \end{bmatrix} = \begin{bmatrix} 0 \\ 0 \end{bmatrix}, \quad (\delta' = w,\ f;\ j = 1,\ 2). \tag{B.6}$$

Equation (B.6) now determines, for each root $\zeta_{\delta' j}$, the ratio of the components $\eta_{x\delta' j}$, $\eta_{z\delta' j}$.

Appendix C

The constant μ^* in Eqs. (18)−(21) is given by

$$\mu^* = \begin{cases} \dfrac{C_{66f}(\Phi)}{2\{1-\nu_f(\Phi)\}}, & (a < h), \\ -\dfrac{2C_{66w}(\Phi)(\kappa_1 + \omega\kappa_2)}{\sin(\pi\omega)}, & (a = h), \end{cases} \tag{C.1}$$

where

$$\nu_f(\Phi) = 2G_{zxf}(\Phi)\left\{\nu_{zxf}(\Phi) + \nu_{yzf}(\Phi)\nu_{xyf}(\Phi)\right\}/E_{xf}(\Phi), \tag{C.2}$$

$$\left.\begin{aligned} \kappa_1 &= \frac{\gamma_1^{2-\omega}(1+\beta_1)\chi_{12} - \gamma_2^{2-\omega}(1+\beta_2)\chi_{11}}{\chi_{11}\chi_{22} - \chi_{12}\chi_{21}}, \\ \kappa_2 &= \frac{\gamma_1^{2-\omega}(1+\beta_1)(\chi_{22}-\chi_{12}) - \gamma_2^{2-\omega}(1+\beta_2)(\chi_{21}-\chi_{11})}{\chi_{11}\chi_{22} - \chi_{12}\chi_{21}}, \end{aligned}\right\} \tag{C.3}$$

$$\left.\begin{aligned} \chi_{1j} &= \{(1+\beta_j)G_0(\Phi) - 2\beta_j\} - 2\{1-\nu_f(\Phi)\}(1+\beta_j)G_0(\Phi)(1+\gamma_j), \\ \chi_{2j} &= \gamma_j\{(1+\beta_j)G_0(\Phi) - 2\} - 2\{1-\nu_f(\Phi)\}(1+\beta_j)G_0(\Phi)(1+\gamma_j), \end{aligned}\right\} \quad (j = 1,\ 2) \tag{C.4}$$

$$\beta_j = \frac{C_{22w}(\Phi)\gamma_j^2 - C_{66w}(\Phi)}{C_{12w}(\Phi) + C_{66w}(\Phi)}, \quad (j = 1,\ 2), \tag{C.5}$$

$$G_0(\Phi) = \frac{C_{66w}(\Phi)}{C_{66f}(\Phi)}, \tag{C.6}$$

and γ_j^2 $(j = 1,\ 2)$ are the roots of the following characteristic equation:

$$C_{22w}(\Phi)C_{66w}(\Phi)\gamma^4 + \left\{C_{12w}(\Phi)^2 + 2C_{12w}(\Phi)C_{66w}(\Phi) - C_{11w}(\Phi)C_{22w}(\Phi)\right\}\gamma^2 + C_{11w}(\Phi)C_{66w}(\Phi) = 0. \tag{C.7}$$

References

[1] S. Kumagai, Y. Shindo, K. Horiguchi and T. Takeda, Mechanical characterization of CFRP woven laminates between room temperature and 4 K, *JSME International Journal Series A*, **46** (2003), 359-364.

[2] J. Ju, R. J. Morgan and T. S. Creasy, Transverse cracking of M40J/PMR-II-50 composites under thermal-mechanical loading: Part I-characterization of main and interaction effects using statistical design of experiments, *Journal of Composite Materials*, **41** (2007), 1009-1031.

[3] A. Nair and S. Roy, Modeling of permeation and damage in graphite/epoxy laminates for cryogenic tanks in the presence of delaminations and stitch cracks, *Composites Science and Technology*, **67** (2007), 2592-2605.

[4] F. Gao, L. Boniface, S. L. Ogin, P. A. Smith and R. P. Greaves, Damage accumulation in woven-fabric CFRP laminates under tensile loading: Part 1. observations of damage accumulation, *Composites Science and Technology*, **59** (1999), 123-136.

[5] B. H. Le Page, F. J. Guild, S. L. Ogin and P. A. Smith, Finite element simulation of woven fabric composites, *Composites : Part A*, **35** (2004), 861-872.

[6] S. Watanabe, Y. Shindo, F. Narita and T. Takeda, Thermal-mechanical analysis of satin weave CFRP composites with cracks at cryogenic temperatures, *Journal of Reinforced Plastics and Composites*, **28** (2009), 1319-1337.

[7] K. Dahlerup-Petersen and A. Perrot, Properties of organic composite materials at cryogenic temperatures, *CERN ISR − BOM*/79 − 39, Geneva, Switzerland, 1979.

[8] N. K. Naik and V. K. Ganesh, Thermo-mechanical behaviour of plain weave fabric composites: experimental investigations, *Journal of Materials Science*, **32** (1997), 267-277.

[9] Z. Hashin, Analysis of properties of fiber composites with anisotropic constituents, *ASME Journal of Applied Mechanics*, **46** (1979), 543-550.

[10] T. C. T. Ting and P. H. Hoang, Singularities at the tip of a crack normal to the interface of an anisotropic layered composite, *International Journal of Solids and Structures*, **20** (1984), 439-454.

[11] M. Stern, Families of consistent conforming elements with singular derivative fields, *International Journal for Numerical Methods in Engineering*, **14** (1979), 409-421.

[12] Advanced Composites Database System: JAXA-ACDB; Ver. 06-1, http://www.jaxa-acdb.com/.

[13] K. Sanada, Y. Shindo and S. Ueda, Stress intensity factors for glass-fiber reinforced plastics with an infinite row of parallel cracks at low temperatures, *Theoretical and Applied Fracture Mechanics*, **28** (1998), 183-196.

[14] S. Kumagai and Y. Shindo, Experimental and analytical evaluation of the notched tensile fracture of CFRP-woven laminates at low temperatures, *Journal of Composite Materials*, **38** (2004), 1151-1164.

Received: January, 2010